# Heavy quark transport in heavy ion collisions at energies available at the BNL Relativistic Heavy Ion Collider and at the CERN Large Hadron Collider within the UrQMD hybrid model

Thomas Lang, Hendrik van Hees, Gabriele Inghirami, Jan Steinheimer, and Marcus Bleicher

Phys. Rev. C **93**, 014901 — Published 5 January 2016

DOI: 10.1103/PhysRevC.93.014901

# Heavy quark transport in heavy ion collisions at RHIC and LHC within the UrQMD hybrid model

Thomas Lang[1], Hendrik van Hees[1,2], Gabriele Inghirami[1,2], Jan Steinheimer[1,2,3], and Marcus Bleicher[1,2]

[1] *Frankfurt Institute for Advanced Studies (FIAS), Ruth-Moufang-Str. 1, 60438 Frankfurt am Main, Germany*

[2] *Institut für Theoretische Physik, Johann Wolfgang Goethe-Universität, Max-von-Laue-Str. 1, 60438 Frankfurt am Main, Germany and*

[3] *Lawrence Berkeley National Laboratory, 1 Cyclotron Road, Berkeley, CA 94720, USA*

## Abstract

We have implemented a Langevin approach for the transport of heavy quarks in the UrQMD hybrid model, which uses the transport model UrQMD to determine realistic initial conditions for the hydrodynamical evolution of the quark gluon plasma (QGP) and the heavy charm and bottom quarks. It provides a realistic description of the background medium for the evolution of relativistic heavy ion collisions. The diffusion of heavy quarks are simulated with a relativistic Langevin approach, using two different sets of drag and diffusion coefficients, one based on a $T$-Matrix approach and one based on a resonance model for the elastic scattering of heavy quarks within the medium. In case of the resonance model we have investigated the effects of different decoupling temperatures of the heavy quarks from the medium, ranging between 130 MeV and 180 MeV. We present calculations of the nuclear modification factor $R_{AA}$, as well as of the elliptic flow $v_2$ in Au+Au collisions at $\sqrt{s_{NN}} = 200$ GeV and Pb+Pb collisions at $\sqrt{s_{NN}} = 2.76$ TeV. To make our results comparable to experimental data at RHIC and LHC we have implemented a Peterson fragmentation and a quark coalescence approach followed by the semileptonic decay of the D- and B-mesons to electrons. We find that our results strongly depend on the decoupling temperature and the hadronization mechanism. At a decoupling temperature of 130 MeV we reach a good agreement with the measurements at both, RHIC and LHC energies, simultaneously for the elliptic flow $v_2$ and the nuclear modification factor $R_{AA}$.

## I. INTRODUCTION

One major goal of ultra-high-energy heavy-ion physics is to recreate the phase of deconfined quarks and gluons (the Quark Gluon Plasma, QGP) as it might have existed a few microseconds after the Big Bang. Various experimental facilities have been built to explore the properties of this QGP experimentally, while on the theory side a multitude of (potential) signatures and properties of the QGP have been predicted [1–3].

Heavy quarks are an ideal probe for the QGP. They are produced in the beginning of the collision in hard processes and therefore probe the created medium during its entire evolution. When the system cools down they hadronize, and their decay products can finally be detected. By investigating heavy-quark observables we can thus explore the interaction processes within the hot and dense medium. Two of the most interesting observables are the nuclear modification factor, $R_{AA}$, and the elliptic flow, $v_2$. Experimentally, the nuclear modification factor shows a large suppression of the open heavy-flavor particles' spectra at high transverse momenta ($p_T$) compared to the findings in pp collisions. This indicates a high degree of thermalization also of the heavy quarks with the bulk medium consisting of light quarks and gluons and perhaps, at the later stages of the fireball evolution, the hot and dense hadron gas. The measured large elliptic flow, $v_2$, of open heavy-flavor mesons and the non-photonic single electrons or muons from their semileptonic decay underlines this interpretation because it indicates that heavy quarks take part in the collective motion of the bulk medium. A quantitative analysis of the degree of thermalization of heavy-quark degrees of freedom in terms of the microscopic scattering processes may lead to an understanding of the mechanisms underlying the large coupling strength of the QGP and the corresponding transport properties.

In this paper we explore the medium modification of heavy-flavor $p_T$ spectra, using a hybrid model, consisting of the Ultra-relativistic Quantum Molecular Dynamics (UrQMD) model [4, 5] and a full (3+1)-dimensional ideal hydrodynamical model [6, 7] to simulate the bulk medium. The heavy-quark propagation in the medium is described by a relativistic Langevin approach [8]. Similar studies have recently been performed in a thermal fireball model with a combined coalescence-fragmentation approach [8–14], in an ideal hydrodynamics model with a lattice-QCD EoS [15, 16], in a model from Kolb and Heinz [17], in the BAMPS model [18, 19], the MARTINI model [20] as well as in further studies and model comparisons [21–25].

The use of hybrid models (as the UrQMD hybrid model used here) provides a major step forward as compared to simplified parametrizations of the temperature and flow. It provides a realistic and well established background, particularly initial conditions for the hydrodynamical evolution of the medium. Additionally, it also includes event-by-event fluctuations and has been shown to describe well many collective properties of relativistic heavy-ion collisions. For the heavy-quark propagation we apply a Langevin approach during the hydrodynamical evolution of the hot and dense medium, employing drag and diffusion coefficients from two effective models for elastic scattering between heavy quarks and light quarks and gluons based on (a) an effective heavy-quark model and the formation of D- or B-meson like resonances in the QGP [26, 27] or (b) a Dirac-Brueckner-$T$-matrix evaluation of the corresponding cross sections based on static heavy-quark potentials from lattice QCD [9]. The hadronization of the heavy quarks to D- or B-mesons is described with a fragmentation or coalescence approach. Within this framework we investigate the effects of using different drag and diffusion coefficients, different freeze-out temperatures of heavy flavors on the heavy-quark observables as well as different hadronization descriptions and compare the results with the experimental data from the Relativistic Heavy Ion Collider (RHIC) and the Large Hadron Collider (LHC).

## II. THE URQMD HYBRID MODEL

To extract information on the interaction of heavy quarks with the medium one ideally applies a well tested model for the (collective) dynamics of the bulk matter. In heavy-ion collisions the medium is by no means homogeneous. Rather it is a locally and event-by-event fluctuating, fast expanding system. In our calculation we employ the state of the art UrQMD hybrid model for the description of the expanding background. This model has been developed in the past years to combine the advantages of hadronic transport theory and ideal fluid dynamics [28]. To account for the non-equilibrium dynamics in the very early stage of the collision in the hybrid model, the UrQMD cascade [4, 5] is used to calculate the initial states of the heavy ion collisions each to be used in a subsequent hydrodynamical evolution [29]. In the present study, the transition from the UrQMD initial state to the hydrodynamical evolution takes place at a time $t = 0.5\,\mathrm{fm}$, which, for RHIC and LHC energies, can be considered an appropriate value to reproduce the bulk properties of the fluid as measured in experiments [30] within hydrodynamical models. The energy, baryon number, and momenta of all particles within UrQMD are mapped onto a spatial grid for the hydrodynamic evolution including event-by-event fluctuations. The full (3+1)-dimensional ideal hydrodynamic evolution is performed using the SHASTA algorithm [6, 7]. We solve the equations for the conservation of energy and momentum and for the conservation of the baryonic charge. With $T^{\mu\nu}$ denoting the relativistic energy-momentum tensor the corresponding equations read

$$\partial_\mu T^{\mu\nu} = 0, \tag{1}$$

and for the baryon four-current $N^\mu$

$$\partial_\mu N^\mu = 0. \tag{2}$$

To transfer all particles back into the UrQMD model, an approximate iso-proper-time transition is chosen (see [31] for details). Here, we apply the Cooper-Frye prescription [32] and transform to particle degrees of freedom via

$$E\frac{\mathrm{d}N}{d^3p} = g_i \int_\sigma \mathrm{d}\sigma_\mu\, p^\mu f(x,p). \tag{3}$$

Here $\mathrm{d}\sigma_\mu = (\mathrm{d}^3x, 0, 0, 0))$ is the hypersurface normal. In Eq. (3) $f(x,p)$ are the Bose- and Fermi-distribution functions and $g_i$ the degeneracy factors for the different particle species. After the "particlization" the evolution proceeds in the hadronic cascade (UrQMD), where final re-scatterings and decays are calculated until all interactions cease and the system decouples. However, since below the decoupling temperature we let the D and B mesons propagate without further hadronic interactions, this final part of the evolution does not affect the $v_2$ and $R_{AA}$ observables. A more detailed description of the hybrid model including parameter tests and results can be found in [28]. A comparison to the results employing the non-approximated hypersurface can be found in [33].

## III. HEAVY-QUARK DIFFUSION

The diffusion of a "heavy particle" in a medium consisting of "light particles" can be described with a Fokker-Planck equation [9, 21, 26, 34–37]. Here one approximates the collision term of the corresponding Boltzmann equation, which in turn can be mapped into an equivalent stochastic Langevin equation.

### A. Relativistic Langevin approach

In the relativistic realm such a Langevin process reads

$$\begin{aligned} \mathrm{d}x_j &= \frac{p_j}{E}\mathrm{d}t, \\ \mathrm{d}p_j &= -\Gamma p_j \mathrm{d}t + \sqrt{\mathrm{d}t} C_{jk}\rho_k. \end{aligned} \tag{4}$$

Here $\mathrm{d}t$ is the time step in the Langevin calculation, $\mathrm{d}x_j$ and $\mathrm{d}p_j$ are the coordinate and momentum changes in each time-step, $E = \sqrt{m^2 + \boldsymbol{p}^2}$, and $\Gamma$ is the drag or friction coefficient. The covariance matrix, $C_{jk}$, of the fluctuating force is related to the diffusion coefficients, as we shall see below. Both $\Gamma$ and $C_{jk}$ depend on $(t, \boldsymbol{x}, \boldsymbol{p})$ and are defined in the (local) rest frame of the fluid. The $\rho_k$ are Gaussian-normal distributed random variables. Their distribution function reads

$$P(\boldsymbol{\rho}) = \left(\frac{1}{2\pi}\right)^{3/2} \exp\left(-\frac{\boldsymbol{\rho}^2}{2}\right) \tag{5}$$

with $\boldsymbol{\rho} = (\rho_1, \rho_2, \rho_3)$. The fluctuating force $F_j^{(\mathrm{fl})}$ thus obeys

$$\left\langle F_j^{(\mathrm{fl})}(t) \right\rangle = 0, \quad \left\langle F_j^{(\mathrm{fl})}(t) F_k^{(\mathrm{fl})}(t') \right\rangle = C_{jl} C_{kl} \delta(t - t'). \tag{6}$$

It is important to note that with these specifications the random process is not yet uniquely determined since one has to specify, at which momentum argument the covariance matrix $C_{jk}$ has to be taken to define the stochastic time integral in (4). As we shall derive now, the demand that the Brownian particle reaches the correct equilibrium-phase-space distribution in the long-time limit of the stochatic process, leads to dissipation-fluctuation relations between the drag and diffusion coefficients [38]. Another approach is to derive the Fokker-Planck equation that is equivalent to the Langevin process as an approximation of the collision term in the Boltzmann equation and adjust the drag coefficient and the covariance matrix accordingly [39]. In the following we derive the Fokker-Planck equation for the heavy-quark phase-space distribution function from the Langevin process defined (4-6) and use the constraint by the correct long-time equilibrium limit to establish the dissipation-fluctuation relations between the drag and diffusion coefficients for different realizations of the Langevin process.

These realizations are defined by the choice of the stochastic integral implied by the contribution of the stochastic force in the momentum-update rule in (4) via a parameter $\xi \in [0, 1]$, determining the momentum argument in the covariance matrix of the white noise, cf. (6)

$$C_{jk} = C_{jk}(t, \boldsymbol{x}, \boldsymbol{p} + \xi \mathrm{d}\boldsymbol{p}). \tag{7}$$

For $\xi = 0$, $\xi = 1/2$, and $\xi = 1$ the corresponding Langevin processes are called the pre-point Ito, the mid-point Stratonovich-Fisk, and the post-point Ito (or Hänggi-Klimontovich) realization, respectively [40].

To derive the Fokker-Planck equation for any choice of $\xi \in [0, 1]$ we consider the time evolution of the average of an arbitrary phase-space function $g(\boldsymbol{x}, \boldsymbol{p})$. To this end we use (4) and (6) with the momentum argument of $C_{jk}$ defined in (7) to derive the time derivative of this expectation value along the stochastic trajectory of the Brownian particle. To this end we need a Taylor expansion with respect to $\mathrm{d}\boldsymbol{x}$ and $\mathrm{d}\boldsymbol{p}$ up to 2$^{\text{nd}}$ order, because the time step is of order $\mathcal{O}(\sqrt{\mathrm{d}t})$ due to the stochastic force:

$$\mathrm{d}g = g(\boldsymbol{x} + \mathrm{d}\boldsymbol{x}, \boldsymbol{p} + \mathrm{d}\boldsymbol{p}) - g(\boldsymbol{x}, \boldsymbol{p}) = \frac{\partial g}{\partial x_j}\mathrm{d}x_j + \frac{\partial g}{\partial p_j}\mathrm{d}p_j + \frac{1}{2}\frac{\partial^2 g}{\partial p_j \partial p_k}\mathrm{d}p_j \mathrm{d}p_k + \mathcal{O}(\mathrm{d}t^{3/2}). \tag{8}$$

Here and in the following we use the Einstein-summation convention, i.e., we sum over repeated indices. Now we have to take the ensemble average of this equation. We consider the three terms on the right-hand side separately, using (4-7):

$$\left\langle \frac{\partial g}{\partial x_j} \mathrm{d}x_j \right\rangle = \left\langle \frac{\partial g}{\partial x_j} \frac{p_j}{E} \mathrm{d}t \right\rangle = \frac{\partial g}{\partial x_j} \frac{p_j}{E} \mathrm{d}t, \tag{9}$$

$$\begin{aligned} \left\langle \frac{\partial g}{\partial p_j} \mathrm{d}p_j \right\rangle &= \left\langle \frac{\partial g}{\partial p_j} \left[ -\Gamma p_j \mathrm{d}t + C_{jk}(\boldsymbol{p} + \xi \mathrm{d}\boldsymbol{p}) \xi_k \sqrt{\mathrm{d}t} \right] \right\rangle \\ &= \left\langle \frac{\partial g}{\partial p_j} \left[ -\Gamma p_j \mathrm{d}t + \left( C_{jk}(\boldsymbol{p}) \rho_k + \frac{\partial C_{jk}(\boldsymbol{p})}{\partial p_l} \xi C_{lm}(\boldsymbol{p}) \rho_k \rho_m \sqrt{\mathrm{d}t} \right) \sqrt{\mathrm{d}t} \right] \right\rangle \\ &\quad + \mathcal{O}(\mathrm{d}t^{3/2}) \\ &= \frac{\partial g}{\partial p_j} \left[ -\Gamma p_j + \xi \frac{\partial C_{jk}(\boldsymbol{p})}{\partial p_l} C_{lk}(\boldsymbol{p}) \right] \mathrm{d}t + \mathcal{O}(\mathrm{d}t^{3/2}) \end{aligned} \tag{10}$$

$$\left\langle \frac{1}{2} \frac{\partial^2 g}{\partial p_j \partial p_k} \mathrm{d}p_j \mathrm{d}p_k \right\rangle = \frac{1}{2} \frac{\partial^2 g}{\partial p_j \partial p_k} C_{jl}(\boldsymbol{p}) C_{kl}(\boldsymbol{p}) \mathrm{d}t + \mathcal{O}(\mathrm{d}t^{3/2}). \tag{11}$$

Combining (9-11), we finally obtain

$$\begin{aligned} \langle g(\boldsymbol{x} + \mathrm{d}\boldsymbol{x}, \boldsymbol{p} + \mathrm{d}\boldsymbol{p}) - g(\boldsymbol{x}, \boldsymbol{p}) \rangle = \Bigg\langle & \frac{\partial g}{\partial x_j} \frac{p_j}{E} + \frac{\partial g}{\partial p_j} \left( -\Gamma p_j + \xi \frac{\partial C_{jk}}{\partial p_l} C_{lk} \right) \\ & + \frac{1}{2} \frac{\partial^2 g}{\partial p_j \partial p_k} C_{jl} C_{kl} \Bigg\rangle \mathrm{d}t + \mathcal{O}(\mathrm{d}t^{3/2}). \end{aligned} \tag{12}$$

Here all momentum arguments of the drag and diffusion coefficients have to be taken at the argument $\boldsymbol{p}$. From (12) via

$$\begin{aligned} \langle g(\boldsymbol{x}, \boldsymbol{p}) \rangle &= \int_{\mathbb{R}^3} \mathrm{d}^3\boldsymbol{x} \int_{\mathbb{R}^3} \mathrm{d}^3\boldsymbol{p} f(t, \boldsymbol{x}, \boldsymbol{p}) g(\boldsymbol{x}, \boldsymbol{p}), \\ \left\langle \frac{\mathrm{d}}{\mathrm{d}t} g(\boldsymbol{x}, \boldsymbol{p}) \right\rangle &= \int_{\mathbb{R}^3} \mathrm{d}^3\boldsymbol{x} \int_{\mathbb{R}^3} \mathrm{d}^3\boldsymbol{p}\, \partial_t f(t, \boldsymbol{x}, \boldsymbol{p}) g(\boldsymbol{x}, \boldsymbol{p}) \\ &\overset{(12)}{=} \int_{\mathbb{R}^3} \mathrm{d}^3\boldsymbol{x} \int_{\mathbb{R}^3} \mathrm{d}^3\boldsymbol{p}\, f(t, \boldsymbol{x}, \boldsymbol{p}) \Bigg[ \frac{\partial g}{\partial x_j} \frac{p_j}{E} + \frac{\partial g}{\partial p_j} \left( -\Gamma p_j + \xi \frac{\partial C_{jk}}{\partial p_l} C_{lk} \right) \\ &\qquad + \frac{1}{2} \frac{\partial^2 g}{\partial p_j \partial p_k} C_{jl} C_{kl} \Bigg] \end{aligned} \tag{13}$$

and integrating by part in the final expression it follows immediately that the time evolution of the phase-space distribution function $f_Q(t, \boldsymbol{x}, \boldsymbol{p})$ of heavy quarks is given by the Fokker-Planck equation,

$$\frac{\partial f_Q}{\partial t} + \frac{p_j}{E} \frac{\partial f_Q}{\partial x_j} = \frac{\partial}{\partial p_j} (A p_j f_Q) + \frac{\partial^2}{\partial p_j \partial p_k} (B_{jl} f_Q), \tag{14}$$

where the coefficients $Ap_j$ and diffusion coefficients,

$$\begin{aligned} & B_{jk} = B_{kj} = B_0 P_{jk}^{\perp} + B_1 P_{jk}^{\|} \\ \text{with} \quad & P_{jk}^{\|} = \frac{p_j p_k}{\boldsymbol{p}^2}, \quad P_{jk}^{\perp} = \delta_{jk} - \frac{p_j p_k}{\boldsymbol{p}^2}. \end{aligned} \tag{15}$$

for an isotropic medium are related to the pertinent parameters in the Langevin process by

$$A p_j = \Gamma p_j - \xi C_{lk} \frac{\partial C_{jk}}{\partial p_l}, \tag{16}$$

$$C_{jk} = \sqrt{2B_0} P_{jk}^{\perp} + \sqrt{2B_1} P_{jk}^{\parallel}. \tag{17}$$

In[1] the case of a background medium in thermal equilibrium ("heat bath"), the stationary limit should become a Boltzmann-Jüttner distribution with the temperature of the "heat bath". Thus, one typically adjusts the drag coefficient by choosing the longitudinal diffusion coefficient, $B_1$, in (17) such as to satisfy this asymptotic equilibration condition [41], leading to dissipation-fluctuation relations between this diffusion coefficient and the drag coefficient [8, 21].

It turns out that for $B_0 = B_1 = D(E)$ and a homogeneous background medium the Boltzmann-Jüttner distribution,

$$f_Q^{(\mathrm{eq})}(\boldsymbol{p}) = \exp\left(-\frac{E}{T}\right), \quad \text{with} \quad E = \sqrt{\boldsymbol{p}^2 + m^2}, \tag{18}$$

becomes a solution of the corresponding stationary Fokker-Planck equation, if the dissipation-fluctuation relation

$$\Gamma(E) E T - D(E) + T(1-\xi) D'(E) = 0, \tag{19}$$

is fulfilled. A straightforward way to achieve the correct asymptotic equilibrium distribution within a relativistic Langevin simulation is to set $\xi = 1$ (i.e., using the post-point Ito realization), which reduces (19) to

$$D(E) = \Gamma(E) E T. \tag{20}$$

For applications to heavy-ion collisions we use $\Gamma$ from underlying microscopic models for heavy-quark scattering with light quarks and gluons as detailed below and adjust the diffusion coefficients $B_0$ (transverse) and $B_1$ (longitudinal) to

$$B_0 = B_1 = \Gamma E T. \tag{21}$$

So far we have defined our Langevin process with respect to the (local) rest frame of the background medium. For a medium with collective flow, one has to evaluate the time step in the local rest frame and boost back to the computational frame. For a closer look on the post-point description see section VII A.

For the heavy-quark propagation in the Langevin model we also need transport coefficients. In this work these drag and diffusion coefficients are obtained from two non-perturbative models for elastic heavy-quark scattering, a resonance model, where the existence of D-mesons and B-mesons in the QGP phase is assumed, as well as a $T$-Matrix approach in which quark-antiquark potentials are used for the calculation of the coefficients in the QGP. They are described in detail in Sec. VII B and are shown in Fig. 1 as function of the three-momentum $|\vec{p}|$ at $T = 180\,\mathrm{MeV}$ and in Fig. 2 as function of the temperature at a fixed three-momentum of $|\vec{p}| = 0.8\,\mathrm{GeV}$. In the appendix VII C we compare the two sets of coefficients used in this article with a third one kindly provided by the Nantes group, based on a Hard-Thermal-Loop model.

[1] In numerical studies it has turned out that drag and diffusion coefficients as obtained from microscopic models usually do not lead to the expected long-time stationary limit of the phase-space distribution for the heavy particles when diffusing in an equilibrated background medium.

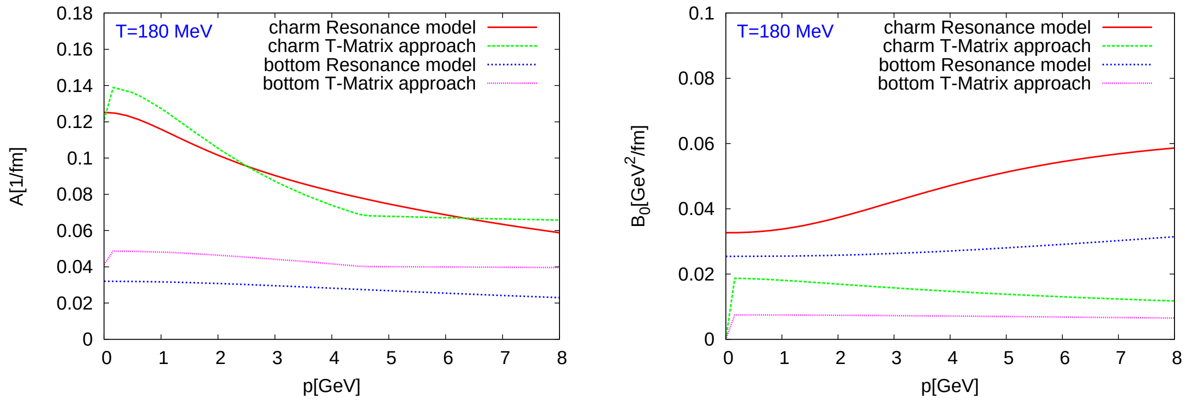


FIG. 1. (Color online) Drag (left) and diffusion (right) coefficients in the resonance model and the T-Matrix approach for charm and bottom quarks. The plot shows the dependence of the coefficients on the three-momentum $|\vec{p}|$ at a fixed temperature of $T = 180\,\text{MeV}$.

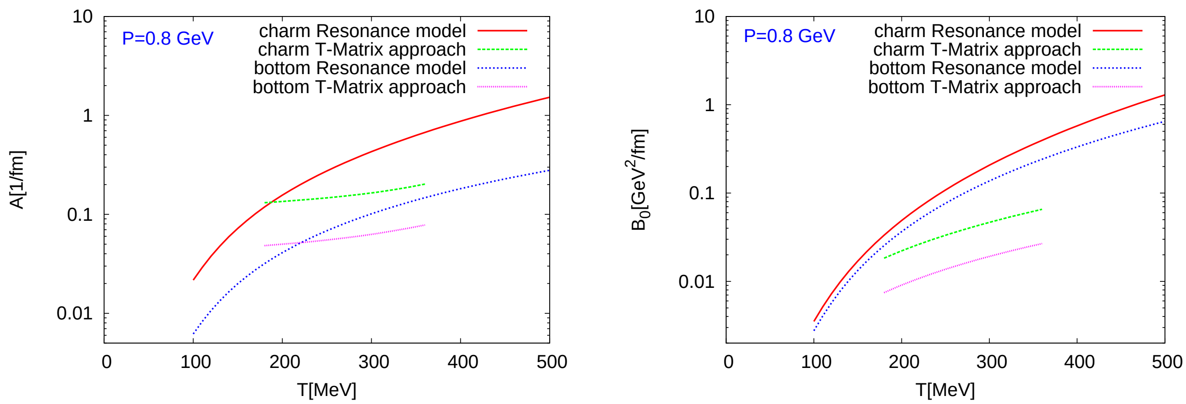


FIG. 2. (Color online) Drag (left) and diffusion (right) coefficients in the resonance model and the T-Matrix approach for charm and bottom quarks. The plot shows the dependence of the coefficients on the temperature at a fixed three-momentum $|\vec{p}| = 0.8\,\text{GeV}$. The T-Matrix coefficients are calculated between $180\,\text{MeV}$ and $360\,\text{MeV}$ only.

### B. Implementation of the Langevin simulation into the UrQMD-hybrid model

For the present study, charm production and propagation is evaluated perturbatively on the time-dependent background generated by the UrQMD/Hybrid model. To model a fluctuating and space-time dependent Glauber-initial state geometry, we perform a first UrQMD run with elastic $0°$ scatterings between the colliding nuclei and save the nucleon-nucleon collision space-time coordinates. These coordinates are used in a second, full UrQMD run as (possible) production coordinates for the heavy quarks.

As momentum distribution for the initially produced charm quarks at $\sqrt{s_{NN}} = 200$ GeV we use

$$\frac{1}{2\pi p_T dp_T} = \frac{(A_1 + p_T)^2}{(1 + A_2 \cdot p_T)^{A_3}}, \tag{22}$$

with $A_1 = 0.5$, $A_2 = 0.1471$ and $A_3 = 21$ and for bottom quarks

$$\frac{1}{2\pi p_T dp_T} = \frac{1}{(A_1 + p_T^2)^{A_2}}, \tag{23}$$

with $A_1 = 57.74$ and $A_2 = 5.04$. These distributions are taken from [9, 27] and are shown in Fig. 3. They are obtained by using tuned c-quark spectra from PYTHIA. Their pertinent semileptonic single-electron decay spectra account for pp and dAu measurements by STAR up to 4 GeV. The missing part at higher $p_T$ is then supplemented by B-meson contributions.

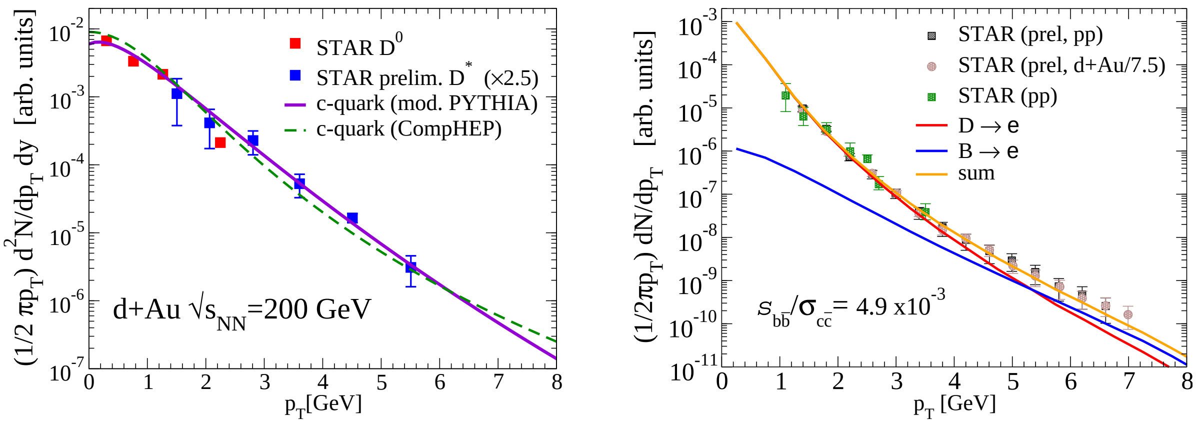


FIG. 3. (Color online) Fits of D- and D*-meson $p_T$ spectra in 200 AGeV d-Au collisions at RHIC with a modified PYTHIA simulation (left panel) and the corresponding non-photonic single-electron $p_T$ spectra in p-p and d-Au collisions (taken from [42]). The missing yield of high-$p_T$ electrons is fitted with the analogous B-meson decay spectra, thus fixing the bottom-to-charm ratio at $\sigma_{b\bar{b}}/\sigma_{c\bar{c}} \simeq 4.9 \cdot 10^{-3}$.

Starting with these charm- and bottom-quark distributions as initial conditions we perform, as soon as the hydrodynamics start condition is fulfilled, an Ito post-point time step of our Langevin simulation as described in Sec. III A, at each time-step of the hydrodynamical evolution.

We use the cell velocities, cell temperatures, the length of the time-step and the $\gamma$-factor of the cells to calculate the momentum transfer, propagating all heavy quarks independently. For the Langevin transport we use the drag and diffusion coefficients obtained from the resonance model or $T$-Matrix approach as described in Sec. VII B.

To analyze the sensitivity of $R_{AA}$ and especially $v_2$ to the decoupling time of the heavy flavors from the medium we vary the decoupling temperatures between 130 MeV and 180 MeV (for the resonance model) and extrapolate the corresponding transport coefficients smoothly into the hadronic phase. This assumption of a smooth transition of the transport coefficients in the transition from the partonic description above and the hadronic one below $T_c$ has been verified, using an effective model for open-heavy-flavor interactions in a hadronic medium in [15, 43].

Our approach provides us with the heavy-quark momentum distribution. We include a hadronization mechanism for open-heavy-flavor mesons (D and B mesons). Since non-photonic single electrons are usually measured in experiments, we perform a semileptonic decay into electrons as final step to compare to data. In addition we also provide D- and B-meson results for direct comparisons to the upcoming direct D/B measurements by the STAR Heavy Flavor Tracker (HFT). These results are shown in Sec. VII D.

## IV. RESULTS AT RHIC ENERGIES

### A. Elliptic flow $v_2$ and nuclear modification factor $R_{AA}$ with fragmentation

Fig. 4 presents the elliptic flow, $v_2$, of charm and bottom quarks from Au+Au collisions at $\sqrt{s_{NN}} = 200$ GeV in the centrality range $\sigma/\sigma_{\text{tot}} = 20\%$-$40\%$ applying a rapidity cut of $|y| < 0.35$.

For our calculation using the drag and diffusion coefficients of the $T$-Matrix model we use a decoupling temperature of 180 MeV, while with the resonance model we show results for decoupling temperatures of 130 MeV, 150 MeV and 180 MeV.

As one can clearly see, the elliptic flow, $v_2$, of bottom quarks (thin lines) is much smaller compared to that of the charm quarks (thick lines) due to their larger mass. Furthermore the use of the coefficients from the $T$-Matrix model compared with those from the resonance model shows that both calculations are in reasonable agreement. The elliptic flow of the charm quarks is nevertheless somewhat lower for the $T$-Matrix model than for the resonance model. When decreasing the decoupling temperature the flow clearly increases. Thus, we conclude that the late phase of the heavy-ion collision may have considerable influence on the heavy-flavor elliptic flow although the drag and diffusion coefficients become small in the late stages of the fireball evolution.

Moreover the $v_2$ is shifted towards higher $p_T$ for lower decoupling temperatures. This effect is due to the increased radial velocity of the medium, which is in case of a developed elliptic flow larger in $x$ than in $y$ direction. Consequently there is a depletion of particles with high $v_x$ in the low $p_T$ region and smaller elliptic flow. This effect is more important for heavier particles and a larger radial flow [44, 45].

To compare our calculations with data on non-photonic electrons from RHIC we perform (in the computational frame) a Peterson fragmentation of the charm and bottom quarks to D-mesons and B-mesons using the fragmentation function from [46],

$$D_Q^H(z) = \frac{N}{z[1-(1/z)-\epsilon_Q/(1-z)]^2},$$

where $N$ is a normalization constant, $z$ the relative-momentum fraction obtained in the fragmentation of the heavy quark and $\epsilon_Q = 0.05(0.005)$ for charm (bottom) quarks [47]. After hadronization we use PYTHIA routines for the semileptonic decay to electrons [48, 49].

Fig. 4 shows our results for the $v_2$ for single electrons in comparison to data from the PHENIX collaboration.

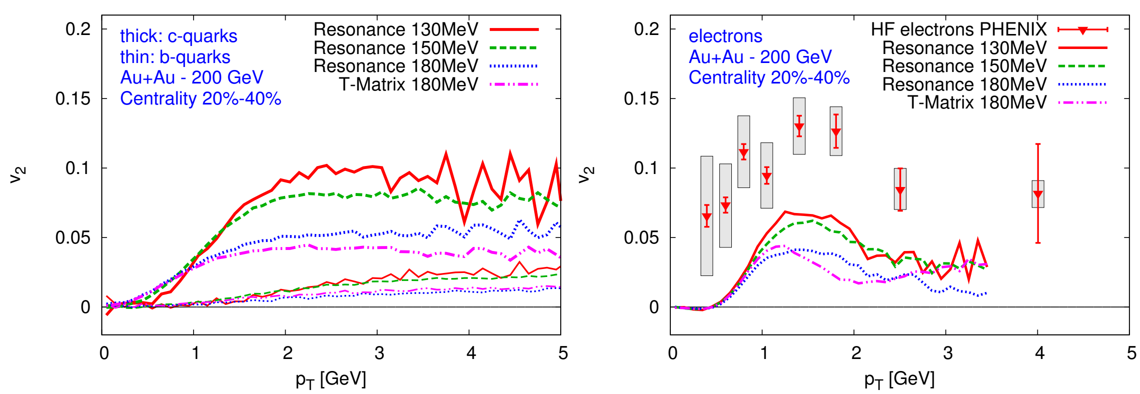


FIG. 4. (Color online) Left: Elliptic flow, $v_2$, of heavy quarks in Au+Au collisions at $\sqrt{s_{NN}} = 200$ GeV. We use a rapidity cut of $|y| < 0.35$. The thick lines depict the charm quarks while the thin lines depict the bottom quarks.
Right: Elliptic flow, $v_2$, of electrons from heavy-meson decays using Peterson fragmentation to D/B mesons and subsequent decay into electrons in Au+Au collisions at $\sqrt{s_{NN}} = 200$ GeV. We use a rapidity cut of $|y| < 0.35$. Data are from [50].

Again we clearly observe the importance of the late phase of the collision. The depletion effect at low $p_T$ described before is clearly visible. The decrease of the elliptic flow at high $p_T$ is due to the increasing fraction of electrons from bottom decays, which have a lower $v_2$ as seen in Fig. 4.

The calculated flow in the setup with the Peterson fragmentation is too small compared to the PHENIX data.

The corresponding nuclear modification factor, $R_{AA}$, for heavy quarks is shown in Fig. 5. Again we present results for Au+Au collisions at $\sqrt{s_{NN}} = 200$ GeV in the centrality range 20%-40%. The quenching for charm quarks is, as expected, much stronger than for bottom quarks. While for bottom quarks the suppression at high $p_T$ is moderate, $R_{AA}$ may drop to 20-30% for charm quarks. The influence of the medium is, as already seen in our flow calculations, larger for a lower decoupling temperature underlining the importance of the late stage of the collision. Fig. 5 shows the comparison of our non-photonic-electron $R_{AA}$ to the data taken by the PHENIX collaboration.

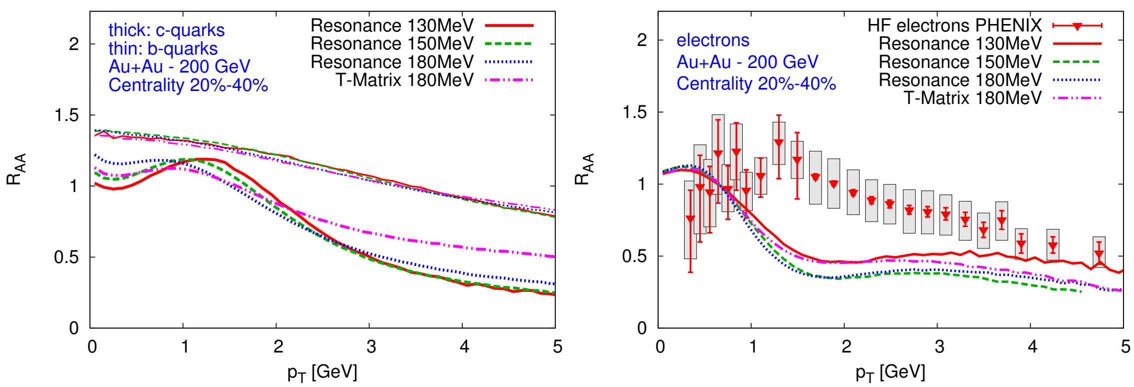


FIG. 5. (Color online) Left: $R_{AA}$ of heavy quarks in Au+Au collisions at $\sqrt{s_{NN}} = 200$ GeV. We use a rapidity cut of $|y| < 0.35$. The thick lines depict the charm quarks while the thin lines depict the bottom quarks.
Right: $R_{AA}$ of electrons from heavy quark decays in Au+Au collisions at $\sqrt{s_{NN}} = 200$ GeV compared to RHIC data [50]. We use a rapidity cut of $|y| < 0.35$. The high-$p_T$ suppression turns out to be too strong compared with the data.

The nuclear modification factor drops quite rapidly and stabilizes at about $p_T \gtrsim 2$ GeV. Around $p_T \approx 2$ GeV it is significantly below the PHENIX data. For higher $p_T$ the calculated $R_{AA}$ approaches the measured data, especially for low decoupling temperatures. This effect is due to the increasing flow of the heavy-flavor particles with decreasing decoupling temperature, which pushes low-$p_T$ heavy-flavor particles towards higher $p_T$ bins.

### Effect of different $\epsilon_Q$ values in the Peterson fragmentation function

To explore the influence of different $\epsilon_Q$ values in the Peterson fragmentation function we show Figures 6. The calculations are performed for the resonance model without modification factor, i.e., with $k = 1$.

One observes that a modification of the epsilon parameter has some influence on the final observables. However, even in this wide range of parameters one is not able to find a parameter that allows to explain both the elliptic flow data and the nuclear modification factor. The problem is that for $\epsilon_Q \to 0$ the edge of the $v_2(p_T)$ and the peak in $R_{AA}$ move to higher $p_T$ values. While the data supports a shift of the $R_{AA}$ peak towards higher $p_T$s (i.e. lower $\epsilon_Q$ values), an improved description of the elliptic flow would benefit from a shift of the edge of the $v_2(p_T)$ towards lower $p_T$.

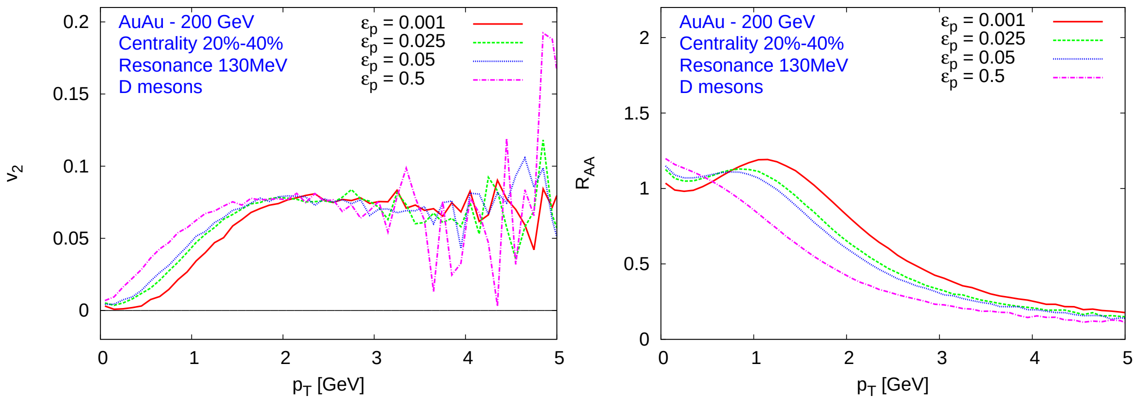


FIG. 6. (Color online) Elliptic flow $v_2$ (left) and $R_{AA}$ (right) of D mesons using different $\epsilon_Q$ values in the Peterson fragmentation function.

### B. Elliptic flow $v_2$ and nuclear modification factor $R_{AA}$ using a $k$ factor

In the previous section we learned that the elliptic flow of the heavy quarks in the calculation with fragmentation is too small compared to experimental data. One possibility to improve on this problem may be to multiply the drag and diffusion coefficients with a "$k$ factor". Therefore we have performed the same calculations as in the last section but using a $k$ factor of 3.

As we see in Fig. 7 the elliptic flow increases considerably due to the stronger coupling of the heavy quarks to the hot medium. The results after performing the Peterson fragmentation and the subsequent decays to electrons are shown in Fig. 7. The elliptic flow is now comparable to the data, especially when using a low decoupling temperature of 130 MeV. Only at low $p_T$ we underestimate the flow due to the depletion effect described above.

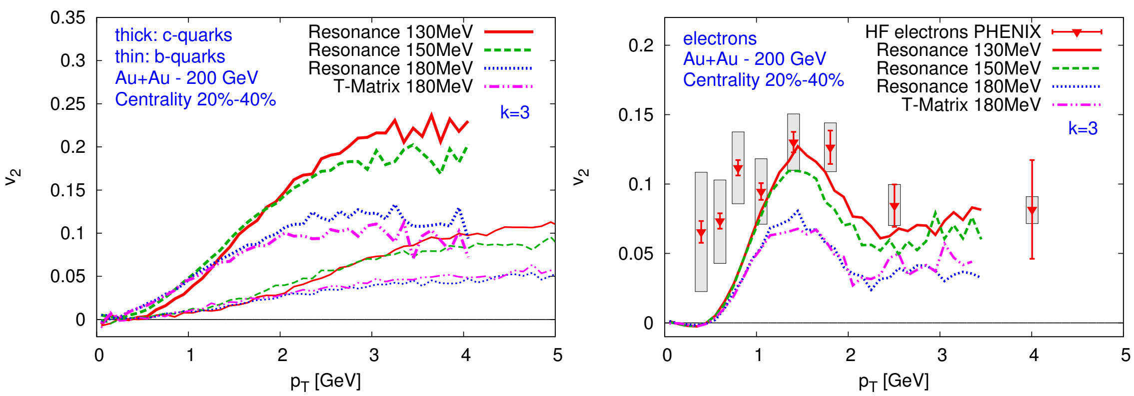


FIG. 7. (Color online) Left: Elliptic flow, $v_2$, of heavy quarks in Au+Au collisions at $\sqrt{s_{NN}} = 200$ GeV employing a $k$ factor of 3. We use a rapidity cut of $|y| < 0.35$. The thick lines depict the charm quarks while the thin lines depict the bottom quarks.
Right: Elliptic flow, $v_2$, of electrons from heavy quark decays in Au+Au collisions at $\sqrt{s_{NN}} = 200$ GeV employing a $k$ factor of 3. We use a rapidity cut of $|y| < 0.35$. The flow in our calculation using a $k$ factor is comparable to data [50].

Our results for the nuclear modification factor, $R_{AA}$, are depicted in Fig. 8. The quenching is much stronger than for the calculation without a $k$ factor. Fig. 8 shows the results for electrons. The suppression of non-photonic electrons at high $p_T$ is also stronger than for the calculation without a $k$ factor.

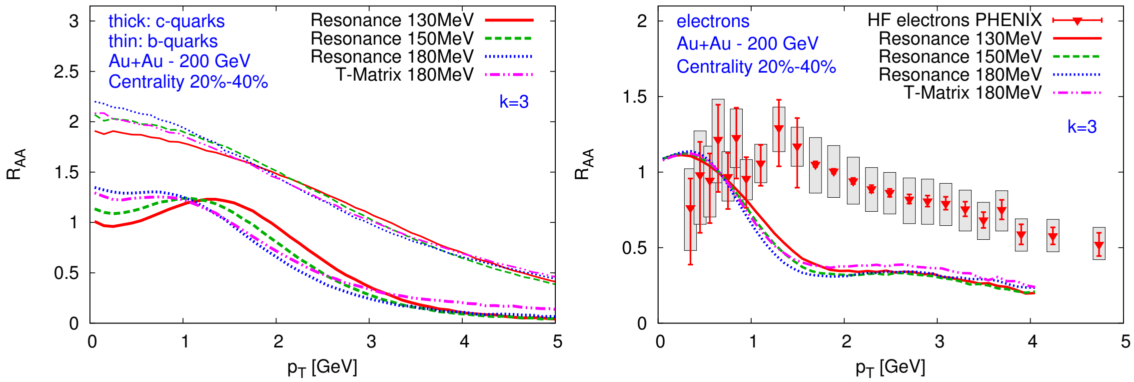


FIG. 8. (Color online) Left: $R_{AA}$ of electrons from heavy-flavor decays in Au+Au collisions at $\sqrt{s_{NN}} =$ 200 GeV employing a $k$ factor of 3. We use a rapidity cut of $|y| < 0.35$. The thick lines show the results for charm quarks and the thin ones for bottom quarks.
Right: $v_2$ of electrons from heavy-flavor decays in Au+Au collisions at $\sqrt{s_{NN}} = 200$ GeV employing a $k$ factor of 3. We use a rapidity cut of $|y| < 0.35$. As expected the medium modification is stronger than without a $k$ factor. Data are taken from [50].

We conclude that the use of a $k$ factor can improve the description of the elliptic flow. However, it is not possible to reach a consistent simultaneous description of both, the elliptic flow and the nuclear modification factor using the same $k$ factor.

### C. Elliptic flow $v_2$ and nuclear modification factor $R_{AA}$ using coalescence

Instead of describing heavy quark hadronization by Peterson fragmentation (and/or an additional k-factor, as discussed above) one can alternatively apply a quark coalescence approach for D- and B-meson production. To implement this coalescence we perform the Langevin calculation until the decoupling temperature is reached. Subsequently we coalesce a light quark with a heavy quark. As the light quarks constitute the medium propagated by hydrodynamics, the average velocities of the light quarks can be (on average) approximated by the flow-velocities of the hydro cells. The mass of the light quarks is assumed to be 370 MeV so that the D-meson mass becomes 1.87 GeV when the masses of the light quarks and the charm quarks (1.5 GeV) are added. Since we assume the light quarks to have the same mass when coalescing with bottom quarks (4.5 GeV), the B-mesons obtain a mass of 4.87 GeV.

The differences of the flow and the spectra of D- and B-mesons when comparing Peterson fragmentation (without $k$-factor) to the coalescence model is shown in Fig. 9. These calculations are performed employing a decoupling temperature of 150 MeV.

As compared to the fragmentation case, the elliptic flow reaches higher values at high $p_T$ due to the coalescence. Also the depletion effect described before is more pronounced. Regarding the nuclear modification factor,the difference of Peterson fragmentation and the coalescence model is even larger. The push of low-$p_T$ particles to higher $p_T$ is stronger in case of the coalescence model, while the suppression of heavy mesons at high $p_T$ is stronger in case of Peterson fragmentation.

Again we perform a decay to electrons using PYTHIA to compare to experimental measurements from the PHENIX collaboration. Fig. 10 (left) shows our results for $v_2$. Due to the coalescence the elliptic flow is strongly increased compared to the previous calculation using the Peterson fragmentation. This higher flow is due to the momentum kick of the light quarks in the recombination process, which provides additional flow from the medium. For a decoupling temperature of

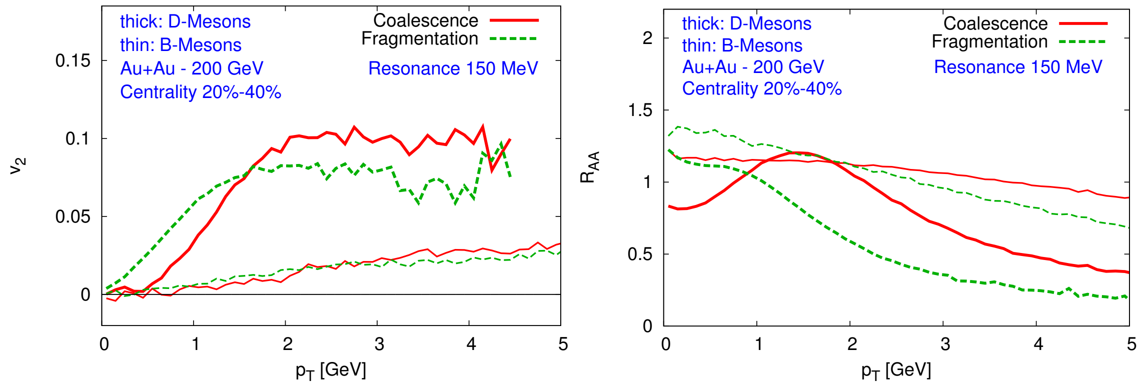


FIG. 9. (Color online) Elliptic flow $v_2$ (left) and $R_{AA}$ (right) of D mesons (thick lines) and B mesons (thin lines) in Au+Au collisions at $\sqrt{s_{NN}} = 200$ GeV. We use a rapidity cut of $|y| < 0.35$. A comparison of a Peterson fragmentation and a coalescence with light quarks is shown. For the drag and diffusion coefficients we use the resonance model with a decoupling temperature of 150 MeV.

130 MeV we obtain a reasonable agreement with the experimental data.

In Fig. 10 (right) the nuclear modification factor for non-photonic single electrons is depicted. Also here we obtain a good agreement with the data. Especially at moderate $p_T \simeq 2$ GeV the

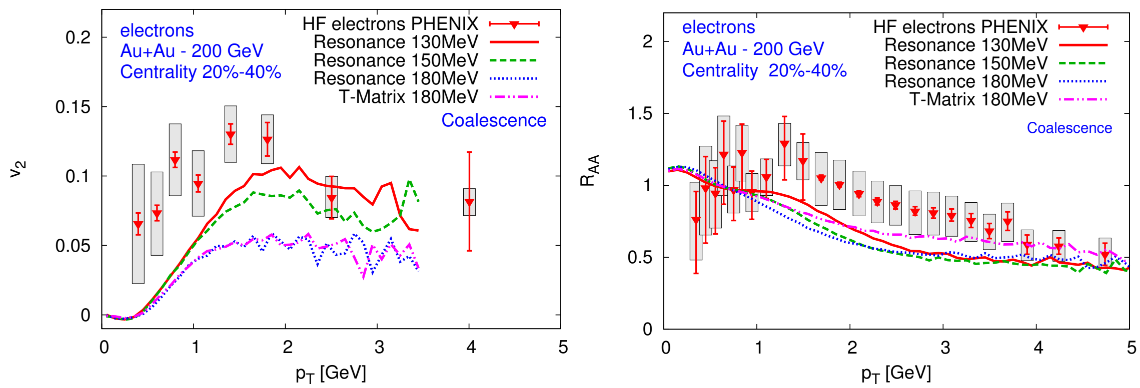


FIG. 10. (Color online) Elliptic flow $v_2$ (left) and nuclear modification factor $R_{AA}$ (right) of electrons from heavy quark decays in Au+Au collisions at $\sqrt{s_{NN}} = 200$ GeV using a coalescence mechanism. We use a rapidity cut of $|y| < 0.35$. For a decoupling temperature of 130 MeV we find a reasonable agreement to data [50].

calculation has strongly improved. The coalescence mechanism pushes the heavy quarks to higher $p_T$. As seen before we obtain the best agreement to data for rather low decoupling temperatures.

In conclusion we observe that the coalescence mechanism is required to describe experimental data with our Langevin model. Only with the coalescence model one is able to describe both $R_{AA}$ and $v_2$ consistently in the present model.

### D. Dependence of the medium modification on the equation of state

The heavy-flavor-flow observables in Langevin simulations are quite sensitive to the used description of the background medium [24]. To examine this issue somewhat further, we have performed our calculations also using different equations of state that are implemented in the UrQMD hybrid model. Our results for different equations of state for the drag and diffusion coefficients of the resonance model with a decoupling temperature of 150 MeV are shown in Fig. 11 for the elliptic flow $v_2$ and for the nuclear modification factor $R_{AA}$.

The equation of state we have been using for all results in the previous sections is the chiral EoS. It is constructed by matching a state of the art hadronic chiral model to a mean-field description of the deconfined phase. The deconfinement transition in this approach is included by the means of an effective Polyakov Loop potential, coupling to the free quarks. It has been shown in [51] that the chiral EoS gives a reasonable description of lattice QCD thermodynamics at $\mu_B = 0$ and can be extended to finite baryon densities. The hadron resonance gas EoS resembles the active degrees of freedom that are also included in the UrQMD transport approach, namely most hadronic states and their resonances. The Bag model EoS [7] follows from matching a Walecka type hadronic model to massless quarks and gluons via a Maxwell construction. It exhibits a strong first order phase transition for all values of $\mu_B$.

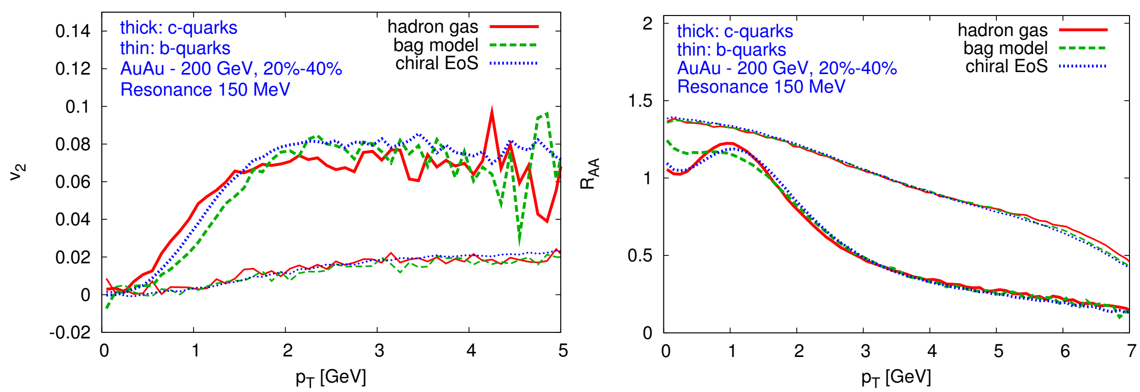


FIG. 11. (Color online) Elliptic flow $v_2$ (left) and nuclear modification factor $R_{AA}$ (right) of heavy quarks in Au+Au collisions at $\sqrt{s_{NN}} = 200$ GeV. We use a rapidity cut of $|y| < 0.35$. Different equations of state are compared.

As one sees clearly the influence on the mediums evolution as seen through the heavy quarks for this set of equations of state is very small.

### E. Averaged initial condition vs. fluctuating initial conditions

While it is long known that the spatial energy density and entropy density distribution is strongly inhomogeneous in the initial state of a heavy ion collision [52] the influence of these inhomogeneities has only been studied systematically in recent years. However, an unambiguous answer whether fluctuating initial conditions (also known as event-by-event initial conditions) for the hydrodynamic stage of the simulation are really needed has become a long standing debate. Previous studies have found that the difference between averaged and fluctuating initial conditions is usually small but depends on the observable under study, see e.g. [53–58].

For the present scenario we compare the results from fluctuating initial conditions with averaged initial conditions in Figure 12. For both heavy quark observable discussed here, i.e., elliptic flow and the nuclear modification factor, we observe only minuscule differences between averaged and fluctuating initial conditions.

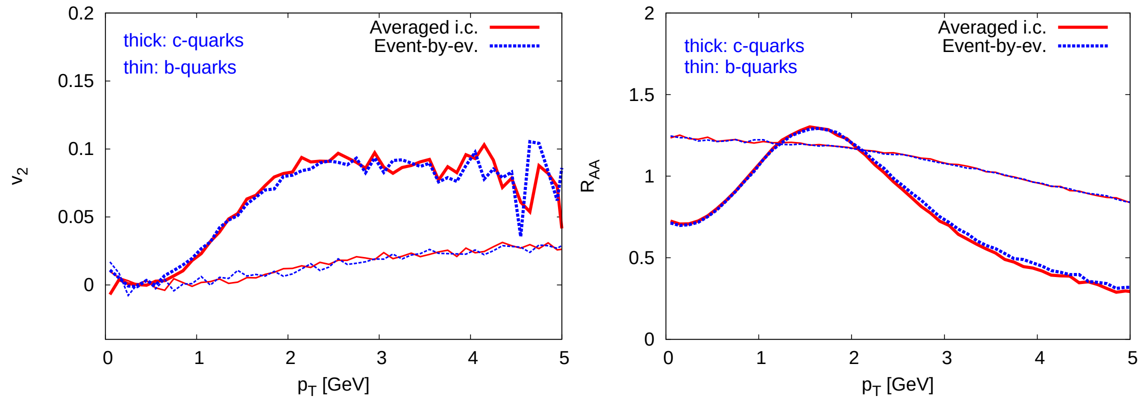


FIG. 12. (Color online) Comparison between calculations with averaged initial conditions to calculations with fluctuating event-by-event initial conditions for the hydrodynamic stage. Left: Elliptic flow $v_2$ of heavy quarks in Au+Au collisions at $\sqrt{s_{NN}} = 200\,\text{GeV}$. Right: Nuclear modification factor $R_{AA}$ of heavy quarks in Au+Au collisions at $\sqrt{s_{NN}} = 200\,\text{GeV}$. The parameters are k=1 and $T_{\text{freeze-out}} = 150$ MeV.

## V. RESULTS AT LHC ENERGIES

In the previous sections we found that we reach the best agreement to experimental PHENIX data when using the resonance model applying a decoupling temperature of 130 MeV and using quark coalescence as hadronization mechanism. Now we apply the same description also at LHC energies ($\sqrt{s_{NN}} = 2.76$ TeV). The momentum distribution for the initially produced charm quarks at LHC is obtained from a fit to PYTHIA calculations. The fit function we use is

$$\frac{\mathrm{d}N}{\mathrm{d}^2 p_T} = \frac{1}{\left(1 + A_1 \cdot \left(p_T^2\right)^{A_2}\right)^{A_3}} \tag{24}$$

with the coefficients $A_1 = 0.136$, $A_2 = 2.055$ and $A_3 = 2.862$.

We have performed our calculations in Pb+Pb collisions at $\sqrt{s_{NN}} = 2.76$ TeV in a centrality range of 30%-50%. The analysis is done in a rapidity cut of $|y| < 0.35$ in line with the ALICE data.

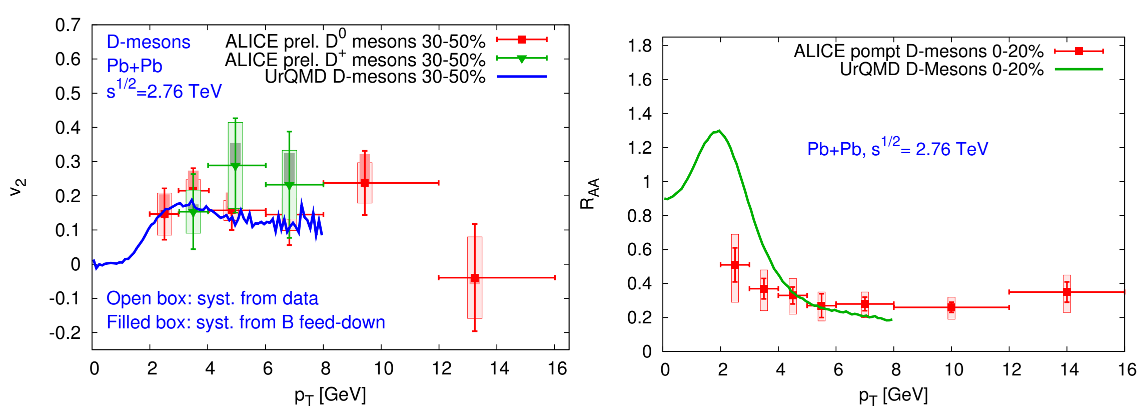


FIG. 13. (Color online) Left: Flow $v_2$ of D-mesons in Pb+Pb collisions at $\sqrt{s_{NN}} = 2.76\,\text{TeV}$ compared to data from the ALICE experiment.[59] A rapidity cut of $|y| < 0.35$ is employed.
Right: $R_{AA}$ of D-mesons in Pb Pb collisions at $\sqrt{s_{NN}} = 2.76$ TeV compared to experimental data from ALICE [60]. A rapidity cut of $|y| < 0.35$ is employed.

Fig. 13 (left) depicts our results for the elliptic flow compared to ALICE measurements. The D-meson $v_2$ exhibits a strong increase and reaches a maximum at about $p_T = 3$ GeV with $v_2 \sim 19\%$. The agreement between the ALICE measurements of $D^0$- and $D^+$-mesons and our calculation is quite satisfactory.

A complementary view on the drag and diffusion coefficients is provided by the nuclear suppression factor $R_{AA}$. Fig. 13 (right) shows the calculated nuclear modification factor $R_{AA}$ of D-mesons at LHC. In line with the experimental data the simulation is done for a more central bin of $\sigma/\sigma_{\rm tot} = 0\%$-$20\%$. We find a maximum of the $R_{AA}$ at about $p_T = 2$ GeV followed by a sharp decline to an $R_{AA}$ of about 0.2 at high $p_T$. As we can see we can describe the data at medium $p_T$ well but over-predict them at low $p_T$ bins.

## VI. SUMMARY

In this paper we have investigated the medium modification of heavy-quark $p_T$ spectra in the hot medium created in heavy-ion collisions at RHIC and LHC energies based on a Langevin simulation for heavy-quark diffusion in the QGP with the hydrodynamical simulation of the "background medium" based on realistic initial conditions for both the bulk medium and the heavy quarks from the UrQMD transport model. The aim of this study was to find a consistent description for both the elliptic flow, $v_2$, and the nuclear modification factor, $R_{AA}$, with a realistic dynamical description of the background medium. We have used two different sets of drag and diffusion coefficients, based on a $T$-Matrix approach and a resonance-scattering model for the elastic scattering of heavy quarks with light quarks and antiquarks. Both sets of coefficients lead to similar results for the heavy-flavor observables.

In the first part of our analysis we have used Peterson fragmentation to describe the hadronization of heavy quarks to open-heavy-flavor mesons.

We have found a low elliptic flow and a too strong heavy-flavor suppression at high $p_T$. Subsequently we have explored how a $k$ factor for the drag and diffusion coefficients would influence the results. We found that with $k = 3$, the description of $v_2$ is improved, but has lead to an even larger suppression of the nuclear modification factor $R_{AA}$, as expected. We conclude that a combination of fragmentation and a Langevin simulation with a $k$-factor in the transport coefficient does not allow for a consistent description of the data on non-photonic single electron spectra in Au+Au collisions ($\sqrt{s_{NN}} = 200$ GeV) at RHIC.

To overcome this problem we have used a coalescence approach to heavy-quark hadronization to open-heavy-flavor mesons instead of the fragmentation. The coalescence mechanism allows for a consistent description of both $v_2$ and $R_{AA}$. We have performed the simulations, assuming different decoupling temperatures of the heavy quarks from the medium, and found that the late phase of the collision can have a considerable effect on the heavy-quark observables. Within our study we find the best agreement to experimental data using a low decoupling temperature of 130 MeV. In Sec. IV D we have also addressed the sensitivity of the heavy-flavor observables to the assumed equation of state of the strongly interacting medium. Here we find that our results are insensitive to variations of the particular equation of state used in UrQMD's hydrodynamic model. Also fluctuations in the initial conditions, simulated with the UrQMD transport model, have an insignificant influence on the heavy-quark observables.

Finally we also explored the medium modification in our model at LHC energies. Here we could reach a good agreement to data for the elliptic flow $v_2$ of D-mesons. For the nuclear modification factor $R_{AA}$ we reach a good agreement at medium $p_T$ but seem to miss the data at low $p_T$ bins.

New complementary measurements with the STAR Heavy Flavor Tracker (HFT) at $\sqrt{s_{NN}} = 200$ GeV are currently in progress. The HFT will enable direct identification of heavy-flavor-meson decays like $D^0 \to K^-\pi^+$ or $D_s^+ \to K^-\pi^+K^+$. This is supposed to lead to better $v_2$ measurements down to very low $p_T$ and a better understanding of the energy loss of heavy quarks in the medium. Especially it will provide us with identified D-meson spectra which will enable us to compare our heavy-meson results to data separately for D- and B-mesons and therefore to get further insights on the hadronization mechanism.

## ACKNOWLEDGMENTS

The authors thank P. B. Gossiaux, M. Nahrgang and J. Aichelin, for providing the set of the drag and diffusion coefficients derived by the Nantes group, and H. Petersen for useful discussions about the simulations with averaged initial conditions. T. Lang and G. Inghirami gratefully acknowledge support from the Helmholtz Research School on Quark Matter Studies and from the Helmholtz Graduate School for Hadron and Ion Research. This work was supported by the Hessian LOEWE initiative through the Helmholtz International Center for FAIR (HIC for FAIR). J. S. acknowledges a Feodor Lynen fellowship of the Alexander von Humboldt foundation. This work was supported by the Office of Nuclear Physics in the US Department of Energy's Office of Science under Contract No. DE-AC02-05CH11231 and the Bundesministerium für Bildung und Forschung (BMBF) grant No. 06FY7083. The computational resources were provided by the Frankfurt LOEWE Center for Scientific Computing (LOEWE-CSC).

## VII. APPENDIX

### A. Post-point Ito realization

Since the phase-space distribution of relativistic particles is a scalar [61], the proper equilibrium limit is given by the corresponding boosted Boltzmann-Jüttner phase-space distribution,

$$f_Q^{(\mathrm{eq})} \propto \exp\left(-\frac{p \cdot u}{T}\right), \tag{25}$$

where $u(t, \boldsymbol{x})$ is the four-velocity field of the medium and $p$ the (on-shell) four-momentum of the heavy quark in the local rest-frame. It can be shown analytically, and we have numerically checked, that for obeying this constraint, one has to apply the post-point prescription, $\xi = 1$, strictly only to the momentum argument of the covariance matrix, $C_{jk}$ as given in (7) and not to the corresponding coefficients originating from the Lorentz transformation of the time step $\mathrm{d}t$ with respect to the laboratory frame (bare symbols) to the one in the local rest-frame of the heat bath (starred symbols), i.e., in the transformation prescription for the time interval,

$$\mathrm{d}t^* = \frac{m}{E^*}\mathrm{d}\tau = \frac{m}{E^*}\frac{E}{m}\mathrm{d}t = \frac{E}{p \cdot u}\mathrm{d}t, \tag{26}$$

one has to use the heavy-quark momenta at time $t$ without a post-point update rule. Here, $\mathrm{d}\tau$ denotes the scalar "proper-time" interval of the heavy quark, corresponding to the given time interval, $\mathrm{d}t$, with respect to the laboratory frame [24].

### B. Drag and diffusion coefficients I

We use two non-perturbative models for elastic heavy-quark scattering in the quark-gluon plasma to evaluate the drag and diffusion coefficients for the Langevin simulation of heavy-quark diffusion.

The resonance model is based on heavy-quark effective theory (HQET) and chiral symmetry in the light-quark sector [26]. Motivated by the finding in lattice-QCD calculations that hadron-like bound states and/or resonances might survive the phase transition in both the light-quark sector (e.g., $\rho$ mesons) and heavy quarkonia (e.g., $J/\psi$), in this model we assume the existence of open-heavy-heavy-flavor meson resonances like the D and B mesons.

In the $T$-Matrix approach static in-medium quark-antiquark potentials from lattice QCD are used as scattering kernels in a Brückner like $T$-matrix approach to calculate the scattering-matrix elements for elastic scattering of heavy quarks with light quarks and antiquarks [9].

The heavy-light quark resonance model[26] is based on the Lagrangian,

$$\begin{aligned}\mathscr{L}_{Dcq} =& \mathscr{L}_D^0 + \mathscr{L}_{c,q}^0 - \mathrm{i}G_S\left(\bar{q}\Phi_0^*\frac{1+\not{v}}{2}c - \bar{q}\gamma^5\Phi\frac{1+\not{v}}{2}c + h.c.\right)\\ &- G_V\left(\bar{q}\gamma^\mu\Phi_\mu^*\frac{1+\not{v}}{2}c - \bar{q}\gamma^5\gamma^\mu\Phi_{1\mu}\frac{1+\not{v}}{2}c + \mathrm{h.c.}\right),\end{aligned} \tag{27}$$

and an equivalent one for bottom quarks. Here $v$ denotes the heavy-quark four-velocity. The free part of the Lagrangian is given by

$$\begin{aligned}\mathscr{L}_{c,q}^0 &= \bar{c}(\mathrm{i}\not{\partial} - m_c)c + \bar{q}\,\mathrm{i}\not{\partial}q,\\ \mathscr{L}_D^0 &= (\partial_\mu\Phi^\dagger)(\partial^\mu\Phi) + (\partial_\mu{\Phi_0}^{*\dagger})(\partial^\mu\Phi_0^*) - m_S^2(\Phi^\dagger\Phi + \Phi_0^{*\dagger}\Phi_0^*)\\ &\quad - \frac{1}{2}(\Phi_{\mu\nu}^{*\dagger}\Phi^{*\mu\nu} + \Phi_{1\mu\nu}^\dagger\Phi_1^{\mu\nu}) + m_V^2(\Phi_\mu^{*\dagger}\Phi^{*\mu} + \Phi_{1\mu}^\dagger\Phi_1^\mu),\end{aligned} \tag{28}$$

where $\Phi$ and $\Phi_0^*$ are pseudo-scalar and scalar meson fields (corresponding to D and $D_0^*$ mesons). Based on chiral symmetry, restored in the QGP phase, we also assume the existence of mass degenerate chiral-partner states. Further from heavy-quark effective symmetry one expects spin independence for both the masses, $m_S = m_V$, and the coupling constants, $G_S = G_V$. For the strange-quark states we take into account only the pseudo-scalar and vector states ($D_s$ and $D_s^*$, respectively).

The D-meson propagators are dressed with the corresponding one-loop self energy. Assuming charm- and bottom-quark masses of $m_c = 1.5$ GeV and $m_b = 4.5$ GeV, we adjust the masses of the physical D-meson-like resonances to $m_D = 2$ GeV and $m_B = 5$ GeV, in approximate agreement with the $T$-matrix models of heavy-light quark interactions in [62, 63]. The coupling constant is chosen such as to obtain resonance widths of $\Gamma_{D,B} = 0.75$ GeV.

With these propagators the elastic $Qq$- and $Q\bar{q}$-scattering matrix elements are calculated and used for evaluation of the pertinent drag and diffusion coefficients for the heavy quarks, using (34) and (35). It turns out that particularly the $s$-channel processes through a D/B-meson like resonance provide a large efficiency for heavy-quark diffusion compared to the pQCD cross sections for the same elastic scattering processes. This results in charm-quark equilibration times $\tau_{\text{eq}}^c$ = 2-10 fm/$c$.

In order to justify the formation of D- and B-meson like resonances above $T_c$, in [9] a Brueckner-like in-medium $T$-matrix approach has been used for the description of elastic heavy-light-quark scattering in the QGP. After a three-dimensional reduction to a Lippmann-Schwinger equation, including a Breit correction, in-medium heavy-quark potentials from lQCD have been employed as the scattering kernels. As an upper limit of the interaction strength within such an approach, the internal-energy potential,

$$U(r,T) = F(r,T) - T\frac{\partial F(r,T)}{\partial T}, \tag{29}$$

has been used, where $F$ is the free-energy potential from the lattice calculation. We take into account also the complete set of $Q\bar{q}$ color states, assuming Casimir scaling of the corresponding potentials,

$$V_8 = -\frac{1}{8}V_1, \quad V_{\bar{3}} = \frac{1}{2}V_1, \quad V_6 = -\frac{1}{4}V_1. \tag{30}$$

After a partial-wave decomposition the Lippmann-Schwinger equation,

$$\begin{aligned} T_{a,l}(E;q',q) = V_{a,l}(q',q) \\ &+ \frac{2}{\pi}\int \mathrm{d}k\; k^2 V_{a,l}(q',k) G_{Qq}(E,k) \\ &\times T_{a,l}(E;k,q)[1 - f_F(\omega_k^Q) - f_F(\omega_k^q)], \end{aligned} \tag{31}$$

for the partial-wave components of each color channel, $a$, has been solved for the $S$- and $P$-wave components. Here, $E$ is the center-of-momentum (CM) energy of the heavy-light quark system, $q$ and $q'$ the momenta of the heavy and light quark, and

$$G_{qQ}(E,k) = \frac{1}{E - (\omega_k^q + \mathrm{i}\Sigma_I^q) - (\omega_k^Q + \mathrm{i}\Sigma_I^Q)} \tag{32}$$

the corresponding two-particle propagator in the CM frame. It has been checked that the quasi-particle widths of $\Gamma_I^{q,Q} = 2\Sigma_I^{q,Q} = 200$ MeV are consistent with a previous similar Br"uckner calculation [64] for the light quarks and with the heavy-quark self-energies with the $T$-matrix solution of (31). The relation with the invariant scattering-matrix elements in (34) is then given by

$$\begin{aligned}\sum|\mathcal{M}|^2 = &\frac{64\pi}{s^2}(s-m_q^2+m_Q^2)^2(s-m_Q^2-m_q^2)^2 \\ &\times N_f \sum_a d_a \left(|T_{a,l=0}(s)|^2 + 3|T_{a,k=1}(s)\cos\theta_{\mathrm{cm}}|^2\right) .\end{aligned} \tag{33}$$

The relation of elastic heavy-quark-scattering matrix elements with the drag and diffusion coefficients in the Langevin approach is given by integrals of the form

$$\begin{aligned}\langle X(\boldsymbol{p}')\rangle = &\frac{1}{2\omega_{\boldsymbol{p}}}\int_{\mathbb{R}^3}\frac{\mathrm{d}^3\boldsymbol{q}}{2E(\boldsymbol{q})\,(2\pi)^3}\int_{\mathbb{R}^3}\frac{\mathrm{d}^3\boldsymbol{p}'}{2E(\boldsymbol{p}')\,(2\pi)^3}\int_{\mathbb{R}^3}\frac{\mathrm{d}^3\boldsymbol{q}'}{2E(\boldsymbol{q}')\,(2\pi)^3}\frac{1}{\gamma_Q}\sum_{g,q}|\mathcal{M}|^2 \\ &\times (2\pi)^4\delta^{(4)}(p+q-p'-q')f_{q,g}(\boldsymbol{q})X(\boldsymbol{p}') .\end{aligned} \tag{34}$$

Here, the integrations run over the three momenta of the incoming light quark or gluon, $\boldsymbol{q}$ and the momenta of the outgoing particles, $\boldsymbol{p}'$ and $\boldsymbol{q}'$. The sum over the matrix element is taken over the spin and color degrees of freedom of both the incoming and outgoing particles; $\gamma_Q = 6$ is the corresponding spin-color degeneracy factor for the incoming heavy quark, and $f_{q,g}$ stands for the Boltzmann distribution function for the incoming light quark or gluon. In this notation, the drag and diffusion coefficients are given by

$$\begin{aligned}A(\boldsymbol{p}) &= \left\langle 1-\frac{\boldsymbol{p}\boldsymbol{p}'}{\boldsymbol{p}^2}\right\rangle , \\ B_0(\boldsymbol{p}) &= \frac{1}{4}\left\langle \boldsymbol{p}'^2-\frac{(\boldsymbol{p}'\boldsymbol{p})^2}{\boldsymbol{p}^2}\right\rangle , \\ B_1(\boldsymbol{p}) &= \frac{1}{2}\left\langle \frac{(\boldsymbol{p}'\boldsymbol{p})^2}{\boldsymbol{p}^2}-2\boldsymbol{p}'\boldsymbol{p}+\boldsymbol{p}^2\right\rangle ,\end{aligned} \tag{35}$$

with the bracket defined by the collision-integral functional (34).

For both approaches we also include the leading-order perturbative QCD cross sections for elastic gluon heavy-quark scattering [65], including a Debye screening mass $m_{Dg} = gT$ in the gluon propagators, thus taming the $t$-channel singularities in the matrix elements. The strong-coupling constant is chosen as $\alpha_s = g^2/(4\pi) = 0.4$.

### C. Drag and diffusion coefficients II

The drag and diffusion coefficients employed in this study are taken from [9, 36]. While the choice of these parameters is well justified, the choice is far from unique. To explore the differences and possibly resulting systematic uncertainties in the observables, we compare the coefficients employed here with the drag and diffusion coefficients derived by the Nantes group see e.g. [66].

Figure 14 shows the comparison between the Nantes coefficients (labeled "HTL") and the coefficients used in the rest of the article, labeled "Resonance" and "$T$-matrix". Here HTL indicates the Nantes coefficients calculated following the definition in [35], while "HTL tuned" corresponds to some tuning of the $B_1$ and $B_0$ coefficients in order to assure that the asymptotic distribution corresponds to Boltzmann Jütner ($A$ is not tuned and kept as is), for details see ref. [67]. The figures indicate that the differences between the drag and diffusion coefficients are substantial (on average more than a factor of two) over all charm momenta.

Let us now compare how these differences influence the finally observed D-meson elliptic flow and the nuclear modification factor. In our numerical simulations we used the HTL coefficients

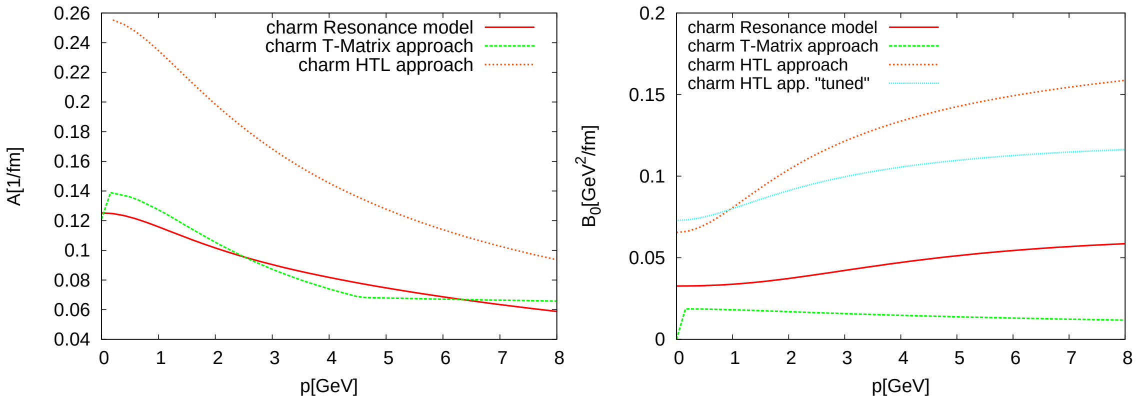


FIG. 14. (Color online) Left: Comparison of the drag coefficients for charm quarks between the Nantes approach ("HTL") and our approach ("T-Matrix","Resonance"). Right: Comparison of the diffusion coefficients for charm quarks between the Nantes approach and our approach.

without any tuning, since the "tuned" ones were computed only up temperatures of 400 MeV. Fig. 16 shows the comparison in detail.

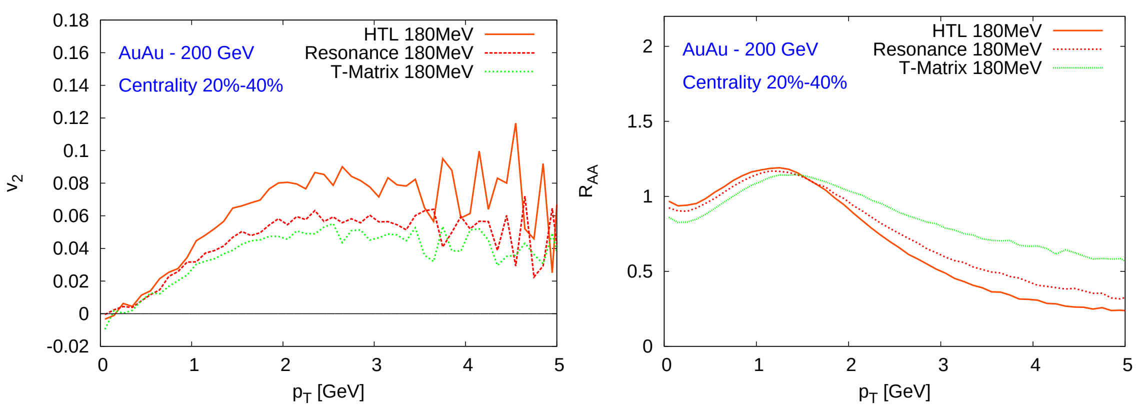


FIG. 15. (Color online) Left: Comparison of the elliptic flows of charm quarks for different drag and diffusion coefficients. Right: Comparison of the nuclear modification factors of charm quarks for different drag and diffusion coefficients. Like in all the previous numerical simulations, even in this case the diffusion coefficients $B_1$ and $B_0$ are computed from the drag coefficient $A$ using (21).

### D. Underlying D- and B-meson spectra before semi-leptonic decays

The heavy flavor electron spectra at RHIC originate from D- and B-meson decays. These D- and B-meson spectra are obtained from our heavy quark calculations applying a fragmentation or a coalescence mechanism. They are displayed in Fig. 17 for the case of the Peterson fragmentation without using a $k$-factor, in Fig. 18 for the case of the Peterson fragmentation applying a $k$-factor of 3 and finally for the case of using a coalescence mechanism (Fig. 19).

These spectra can act as a prediction for future D- and B-meson measurements at RHIC energies. On the one hand they allow for a comparison of our hadronization mechanisms to experimental data and on the other hand for a comparison of the decay to heavy flavor electrons performed using PYTHIA.

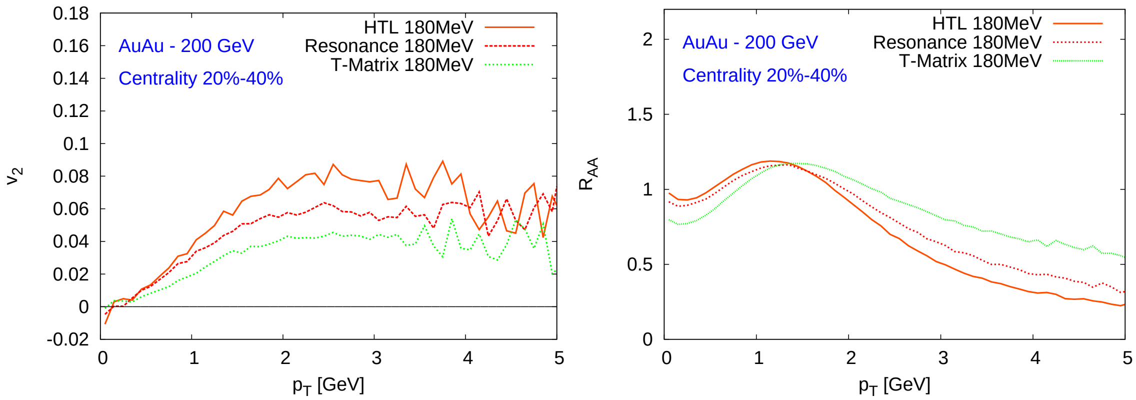


FIG. 16. (Color online) Left: Comparison of the elliptic flows of charm quarks for different drag and diffusion coefficients. Right: Comparison of the nuclear modification factors of charm quarks for different drag and diffusion coefficients. In the numerical simulations performed to produce these plots only the $B_1$ coefficients are computed from the $A$ coefficients using 21, while the $B_0$ coefficients are taken from the underlying models for the HQ scattering cross sections.

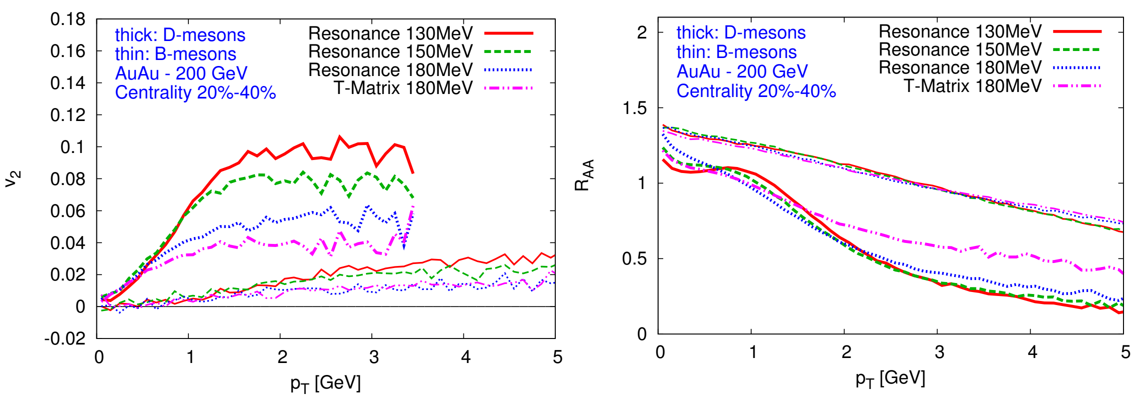


FIG. 17. (Color online) Elliptic flow $v_2$ (left) and nuclear modification factor $R_{AA}$ (right) of D- and B-mesons using Peterson fragmentation in Au+Au collisions at $\sqrt{s_{NN}} = 200\,\text{GeV}$. We use a rapidity cut of $|y| < 0.35$.

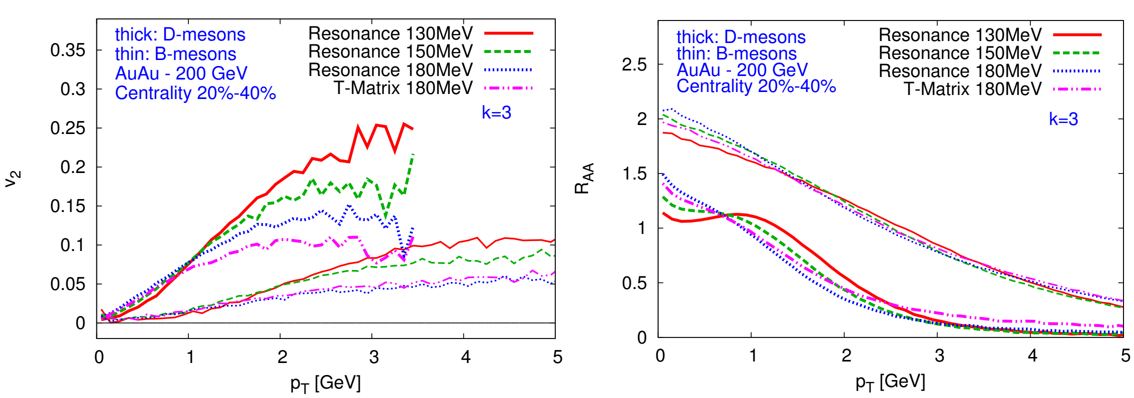


FIG. 18. (Color online) Elliptic flow $v_2$ (left) and nuclear modification factor $R_{AA}$ (right) of D- and B-mesons using Peterson fragmentation and a k-factor of 3 in Au+Au collisions at $\sqrt{s_{NN}} = 200\,\text{GeV}$. We use a rapidity cut of $|y| < 0.35$.

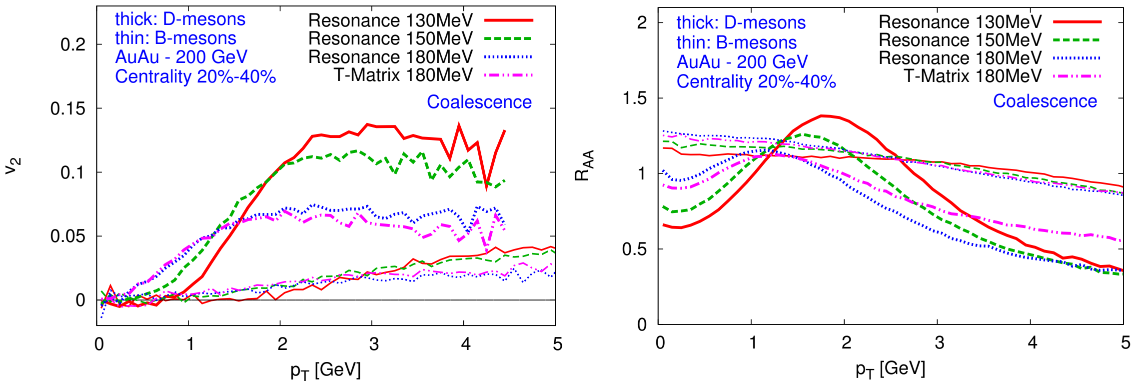


FIG. 19. (Color online) Elliptic flow $v_2$ (left) and nuclear modification factor $R_{AA}$ (right) of D- and B-mesons using coalescence in Au+Au collisions at $\sqrt{s_{NN}} = 200\,\mathrm{GeV}$. We use a rapidity cut of $|y| < 0.35$.

[1] J. Adams *et al.* (STAR Collaboration), Nucl. Phys. A **757**, 102 (2005), arXiv:nucl-ex/0501009 [nucl-ex].
[2] K. Adcox *et al.* (PHENIX Collaboration), Nucl. Phys. A **757**, 184 (2005), arXiv:nucl-ex/0410003 [nucl-ex].
[3] B. Müller, J. Schukraft, and B. Wyslouch, Ann. Rev. Nucl. Part. Sci. **62**, 361 (2012).
[4] S. Bass, M. Belkacem, M. Bleicher, M. Brandstetter, L. Bravina, *et al.*, Prog. Part. Nucl. Phys. **41**, 255 (1998).
[5] M. Bleicher, E. Zabrodin, C. Spieles, S. Bass, C. Ernst, *et al.*, J. Phys. G **25**, 1859 (1999).
[6] D. H. Rischke, S. Bernard, and J. A. Maruhn, Nucl. Phys. A **595**, 346 (1995).
[7] D. H. Rischke, Y. Pursun, and J. A. Maruhn, Nucl. Phys. A **595**, 383 (1995).
[8] R. Rapp and H. van Hees, (2009), published in R. C. Hwa, X.-N. Wang (Ed.), Quark Gluon Plasma 4, World Scientific, p. 111, arXiv:0903.1096 [hep-ph].
[9] H. van Hees, M. Mannarelli, V. Greco, and R. Rapp, Phys. Rev. Lett. **100**, 192301 (2008).
[10] H. van Hees, V. Greco, and R. Rapp, (2007), arXiv:0706.4456 [hep-ph].
[11] V. Greco, H. van Hees, and R. Rapp, (2007), arXiv:0709.4452 [hep-ph].
[12] H. van Hees, M. Mannarelli, V. Greco, and R. Rapp, Eur. Phys. J. **61**, 799 (2009).
[13] R. Rapp, D. Cabrera, V. Greco, M. Mannarelli, and H. van Hees, (2008), arXiv:0806.3341 [hep-ph].
[14] R. Rapp and H. van Hees, (2008), published in The Physics of Quarks: New Research, Nova Publishers (Horizons in World Physics, Vol. 265) (2009), arXiv:0803.0901 [hep-ph].
[15] M. He, R. J. Fries, and R. Rapp, Phys. Rev. Lett. **110**, 112301 (2013).
[16] M. He, R. J. Fries, and R. Rapp, Nucl. Phys. A **910-911**, 409 (2013).
[17] J. Aichelin, P. B. Gossiaux, and T. Gousset, Acta Phys. Polon. B **43**, 655 (2012).
[18] J. Uphoff, O. Fochler, Z. Xu, and C. Greiner, Phys. Rev. C **84**, 024908 (2011).
[19] J. Uphoff, O. Fochler, Z. Xu, and C. Greiner, Phys. Lett. B **717**, 430 (2012).
[20] C. Young, B. Schenke, S. Jeon, and C. Gale, Phys. Rev. C **86**, 034905 (2012).
[21] G. D. Moore and D. Teaney, Phys. Rev. C **71**, 064904 (2005).
[22] I. Vitev, A. Adil, and H. van Hees, J. Phys. G **34**, S769 (2007).
[23] P. Gossiaux, J. Aichelin, T. Gousset, and V. Guiho, J. Phys. G **37**, 094019 (2010).
[24] P. B. Gossiaux, S. Vogel, H. van Hees, J. Aichelin, R. Rapp, M. He, and M. Bluhm, Phys. Rev. C (2011).
[25] P. Gossiaux, J. Aichelin, and T. Gousset, Prog. Theor. Phys. Suppl. **193**, 110 (2012).
[26] H. van Hees and R. Rapp, Phys. Rev. C **71**, 034907 (2005).
[27] H. van Hees, V. Greco, and R. Rapp, Phys. Rev. C **73**, 034913 (2006).
[28] H. Petersen, J. Steinheimer, G. Burau, M. Bleicher, and H. Stöcker, Phys. Rev. C **78**, 044901 (2008).
[29] J. Steinheimer, M. Bleicher, H. Petersen, S. Schramm, H. Stöcker, *et al.*, Phys. Rev. C **77**, 034901 (2008).
[30] H. Petersen, C. Coleman-Smith, S. A. Bass, and R. Wolpert, J. Phys. G **38**, 045102 (2011).
[31] Q. feng Li, J. Steinheimer, H. Petersen, M. Bleicher, and H. Stöcker, Phys. Lett. B **674**, 111 (2009).
[32] F. Cooper and G. Frye, Phys. Rev. D **10**, 186 (1974).
[33] P. Huovinen and H. Petersen, Eur. Phys. J. A **48**, 171 (2012).
[34] B. Svetitsky, Phys. Rev. D **37**, 2484 (1988).
[35] M. Golam Mustafa, D. Pal, and D. Kumar Srivastava, Phys. Rev. C **57**, 889 (1998).
[36] H. van Hees, V. Greco, and R. Rapp, Phys. Rev. C **73**, 034913 (2006).
[37] P. B. Gossiaux and J. Aichelin, Phys. Rev. C **78**, 014904 (2008).
[38] P. B. Arnold, Phys. Rev. E **61**, 6091 (2000).
[39] M. He, H. van Hees, P. B. Gossiaux, R. J. Fries, and R. Rapp, Phys. Rev. E **88**, 032138 (2013).
[40] J. Dunkel and P. Hänggi, Physics Reports **471**, 1 (2009).
[41] M. He, H. van Hees, P. B. Gossiaux, R. J. Fries, and R. Rapp, Phys. Rev. E **88**, 032138 (2013).
[42] R. Rapp, V. Greco, and H. van Hees, Nucl. Phys. A **774**, 685 (2006).
[43] M. He, R. J. Fries, and R. Rapp, Phys. Lett. B **701**, 445 (2011).
[44] P. Huovinen, P. Kolb, U. W. Heinz, P. Ruuskanen, and S. Voloshin, Phys. Lett. B **503**, 58 (2001).
[45] D. Krieg and M. Bleicher, Eur. Phys. J. A **39**, 1 (2009).
[46] C. Peterson, D. Schlatter, I. Schmitt, and P. M. Zerwas, Phys. Rev. D **27**, 105 (1983).
[47] J. Chrin, Z. Phys. C **36**, 163 (1987).

[48] T. Sjostrand, S. Mrenna, and P. Z. Skands, JHEP **0605**, 026 (2006).
[49] T. Sjostrand, S. Mrenna, and P. Z. Skands, Comput. Phys. Commun. **178**, 852 (2008).
[50] A. Adare *et al.* (PHENIX Collaboration), Phys. Rev. C **84**, 044905 (2011).
[51] J. Steinheimer, S. Schramm, and H. Stöcker, Phys. Rev. C **84**, 045208 (2011).
[52] M. Bleicher, L. Gerland, C. Spieles, A. Dumitru, S. Bass, *et al.*, Nucl. Phys. A **638**, 391 (1998).
[53] H.-J. Drescher and Y. Nara, Phys. Rev. C **76**, 041903 (2007).
[54] B. Tavares, H.-J. Drescher, and T. Kodama, Braz. J. Phys. **37**, 41 (2007).
[55] R. Andrade, A. dos Reis, F. Grassi, Y. Hama, W. Qian, *et al.*, Acta Phys. Polon. B **40**, 993 (2009).
[56] R. Andrade, F. Grassi, Y. Hama, T. Kodama, and W. Qian, Phys. Rev. Lett. **101**, 112301 (2008).
[57] H. Petersen and M. Bleicher, Phys. Rev. C **79**, 054904 (2009).
[58] H. Petersen and M. Bleicher, Phys. Rev. C **81**, 044906 (2010).
[59] Z. C. del Valle, Nuclear Physics A **904905**, 178c (2013), the Quark Matter 2012 Proceedings of the {XXIII} International Conference on Ultrarelativistic NucleusNucleus Collisions.
[60] B. Abelev *et al.* (ALICE Collaboration), JHEP **1209**, 112 (2012), arXiv:1203.2160 [nucl-ex].
[61] S. R. de Groot, W. A. van Leeuwen, and C. G. van Weert, *Relativistic kinetic theory: principles and applications* (North-Holland, 1980).
[62] D. Blaschke, G. Burau, T. Barnes, Y. Kalinovsky, and E. Swanson, Heavy Ion Phys. **18**, 49 (2003).
[63] D. Blaschke, G. Burau, Y. L. Kalinovsky, and V. L. Yudichev, Prog. Theor. Phys. Suppl. **149**, 182 (2003).
[64] M. Mannarelli and R. Rapp, Phys. Rev. C **72**, 064905 (2005).
[65] B. L. Combridge, Nucl. Phys. B **151**, 429 (1979).
[66] M. Nahrgang, J. Aichelin, P. B. Gossiaux, and K. Werner, Phys. Rev. C **90**, 024907 (2014).
[67] P. B. Gossiaux, V. Guiho, and J. Aichelin, J. Phys. G **31**, S1079 (2005).